Satellite spectra for heliumlike titanium

F. Bely-Dubau, P. Faucher, and L. Steenman-Clark
Observatoire de Nice, Bôite Postale No. 252, 06007 Nice Cedex, France

M. Bitter, S. von Goeler, and K. W. Hill
Plasma Physics Laboratory, Princeton University, Princeton, New Jersey 08544

C. Camhy-Val
Unité d'Enseignement et de Recherche Physique, Université de Paris VII, 75005 Paris, France

J. Dubau
Observatoire de Meudon, 92190 Meudon, France
(Received 25 May 1982)

Wavelengths and atomic parameters for both dielectronic and inner-shell satellite lines of the type $1s^2nl$-$1s2l'nl''$, with $n=2$, 3, and 4, have been calculated for Ti^{19+}. The atomic data were calculated in a multiconfiguration intermediate-coupling scheme and are compared with previous results for $n=2$. The intensities of the higher-n satellites are derived from these data and thus an estimate of the contribution of the unresolved dielectronic satellites to the resonance line is obtained. Direct excitation rates are also given for the resonance, intercombination, and forbidden lines for He-like titanium. Cascades and the effect of resonances for these lines are not considered in this paper. These results are used to fit an experimental soft-x-ray spectrum from the Poloidal Divertor Experiment tokamak discharge. Good agreement is obtained between computed and observed spectra.

I. INTRODUCTION

The study of the H- and He-like resonance-line satellites provides a convenient method for spectroscopic diagnosis of both astrophysical and laboratory plasmas at high temperatures.[1–3] Satellite lines, for example, to the He-like $1s^2$-$1s2l'$ parent line, are due to transitions of the type

$$1s^2nl - 1s2l'nl'', \quad \text{with } n \geq 2 . \tag{1.1}$$

High-resolution spectra ($\lambda/\Delta\lambda > 1000$) for these inner-shell transitions in highly ionized atoms have been first observed from solar active regions[4] and flares.[5] During the maximum solar activity, many such soft-x-ray spectra were obtained from spectrometers aboard spacecraft: SOLFLEX flown by Naval Research Laboratory[6]; XRP on the Solar Maximum Mission.[7]

Recently, high-resolution satellite spectra have been observed from tokamak plasma discharges.[8–10] Tokamak plasmas are the best diagnosed low-density high-temperature plasmas and are therefore suitable sources for the comparison of observed wavelengths and line intensities with results from sophisticated calculations. Tokamaks contain spurious amounts ($<0.1\%$) of high-Z elements. These elements enter the plasma as impurities from the walls of the vacuum vessel and the plasma limiters, or are introduced for diagnostic purposes. Most abundant are iron, chromium, nickel, the constituents of the stainless-steel walls of the vacuum vessel, and titanium which is frequently used as a getter. The high-Z elements are only partially ionized in the hot core of tokamak discharges and occur predominantly in the He- and H-like ion states for central electron temperatures in the range from 1 to 10 keV. The radiation emitted from these ions is therefore of great interest for determination of the central plasma parameters. These diagnostic applications include measurements of the central ion temperature from the Doppler broadening of spectral lines as well as measurements of the central electron temperature, the ionization equilibrium and impurity transport from intensity ratios. Doppler broadening measurements of high-Z impurity x-ray lines are particularly important as an ion-temperature diagnostic for future large-size tokamaks.

 ©1982 The American Physical Society

This paper presents the calculations for Ti carried out for all the He-like resonance-line satellites corresponding to the transitions represented by Eq. (1.1) for $n=2$, 3, and 4. The physical processes considered are those of dielectronic capture and inner-shell excitation for $n=2$. Cascade transitions are not taken into account. For $n \geq 5$, the wavelengths and intensities of the dielectronic satellite lines have been extrapolated using the methods developed in preceding papers.[11–14] These satellites (as well as a large number of the $n=3,4$ satellites) are blended with the resonance line. Theoretical contributions of the unresolved satellite lines are given as a function of the temperature for a spectral resolution which corresponds to a Doppler resolution at 15×10^6 K.

Calculations are also given for direct excitation rates of the He-like lines corresponding to the transitions $1s^2$-$1s2l$. The autoionizing resonances are not included in the calculations. As discussed by Bely-Dubau *et al.*[14] for Fe^{24+}, these effects may be negligible for certain lines from such highly ionized atoms.

These theoretical results have been used to fit successfully a high-resolution spectrum of Ti between 2.605 Å and 2.615 Å observed in PDX (Poloidal Divertor Experiment) tokamak discharges. This spectral range corresponds to the Ti^{20+} resonance line as well as the corresponding satellite lines with $n>2$. Comparison between theoretical and experimental results enables a small correction to the theoretical wavelengths with $n=3$ and 4 to be made. This correction is used to obtain a better extrapolation for the higher-n satellite lines. The Doppler and electron temperatures of the plasma thus deduced from the fitting are in good agreement with those obtained from other methods.

III. DIELECTRONIC SATELLITE LINES

The expression for the intensity I_{sf} of a satellite line, populated by dielectronic recombination from a level s to a level f, relative to the intensity I_R of the resonance line populated by direct excitation, has been discussed in detail by Gabriel,[3] Bely-Dubau *et al.*,[11] Dubau *et al.*,[15] and can be expressed as

$$I_{sf}/I_R = F_1(T_e)F_2(sf) \ . \tag{2.1}$$

The dependence on the electron temperature T_e in (2.1) is collected in the function $F_1(T_e)$ which, from Bely-Dubau *et al.*[13] can be written

$$F_1(T_e) = \frac{2.07\times10^{-16}}{C(T_e)}\frac{1}{g_1}\frac{\exp(-E_s/kT_e)}{T_e^{3/2}} \ , \tag{2.2}$$

where g_1 is the statistical weight of the He-like ground state, C is the collisional excitation rate for the resonance line, and E_s is the energy of the satellite level s with respect to the He-like ground state. The values of E_s for the $n\geq4$ satellites are obtained assuming the hydrogenic approximation:

$$E_s(1s2l'nl) = E_R - R\frac{(Z-2)^2}{n^2} \ , \tag{2.3}$$

where R is the Rydberg constant, Z is the ion charge, and E_R is the energy of the resonance line ($E_R=4.753$ keV). For $n=2$ and 3, we have adopted the following mean values obtained from the program SUPERSTRUCTURE[16]: $E_2=3.311$ and 4.141 keV, respectively. It should be noted that the function $F_1(T_e)$ varies as T_e^{-1} in the temperature range of interest. $F_2(sf)$ is a function dependent only on the atomic parameters of the satellite line and is as follows:

$$F_2(sf) = \frac{g_s A_a^s A_r^{sf}}{\sum_{k<s} A_r^{sk} + A_a^s} \ , \tag{2.4}$$

where A_a^s and A_r^{sf} are the autoionization and radiative transition probabilities in s^{-1}, and g_s is the statistical weight of the level s. The satellite levels s can also be populated by radiative cascades from higher excited levels. This effect was considered by Dubau *et al.*[15] As this effect is small for the satellite lines considered in this paper, this population mechanism is neglected.

The atomic parameters, energy, autoionizing rate (A_a), and radiative decay rate (A_r), have been calculated for all the transitions represented by process (1.1) for values of n equal to 2, 3, and 4. The method used involves the program SUPERSTRUCTURE[16] and the associated DISTORTED WAVE program and follows the procedure described in Bely-Dubau *et al.*[11] These programs use a parametric Thomas-Fermi-Dirac potential $V(\lambda_l,r)$. The values of λ_l for $l=0$, 1, 2 were obtained using a minimization procedure described by Steenman-Clark *et al.*[17] The values obtained for λ_s, λ_p, and λ_d are 2.379, 1.636, and 1.932, respectively. The results are derived in full intermediate coupling and are shown in Tables I and II, for $n=2$, 3, and 4. Also tabulated are the line factors $F_2(sf)$ which are directly related to the intensities due to dielectronic recombination. In Table I, the lines are defined using the same no-

TABLE I. Atomic data related to all the satellite lines due to the complex $n=2$ compared with data of Bhalla *et al.* (Ref. 18) and Vainshtein and Safronova (Ref. 19). The corrected wavelengths are in Å. Radiative probabilities A_r^{sf}, $\sum_{k<s} A_r^{sk}$, autoionization rates A_a^s, and line factors $F_2(sf)$ are in units of 10^{13} s^{-1}.

									Bhalla *et al.*			Vainshtein and Safronova		
Array	Multiplet	Line	Key	λ (Å)	A_r^{sf}	$\sum_{k<s} A_r^{sk}$	A_a^s	$F_2(sf)$	λ (Å)	A_r^{sf}	A_a^s	λ (Å)	A_r^{sf}	A_a^s
$1s^2 2p$-$1s\,2p^2$	$^2P^o$-^2P	$\frac{3}{2}$-$\frac{3}{2}$	*a*	2.6293	32.06	33.37	2.104	7.608	2.6295	35.2	1.5	2.6295	32.0	2.8
		$\frac{1}{2}$-$\frac{3}{2}$	*b*	2.6243	1.297	33.37	2.104	3.078(−1)	2.6253	1.98	1.5	2.6253	1.07	2.8
		$\frac{3}{2}$-$\frac{1}{2}$	*c*	2.6338	9.212	35.94	4.390(−1)	2.22(−2)	2.6339	9.87	2.39(−2)	2.6341	9.23	4.74(−2)
		$\frac{1}{2}$-$\frac{1}{2}$	*d*	2.6291	26.85	35.94	4.390(−1)	6.552(−2)	2.6297	29.1	2.39(−2)	2.6299	26.8	4.74(−2)
	$^2P^o$-^4P	$\frac{3}{2}$-$\frac{5}{2}$	*e*	2.6455	6.347(−1)	6.353(−1)	8.448(−1)	2.174	2.6451	8.35(−1)	9.76(−1)	2.6450	6.7(−1)	1.02
		$\frac{3}{2}$-$\frac{3}{2}$	*f*	2.6480	2.001(−1)	2.034(−1)	7.125(−2)	2.077(−1)	2.6474	2.16(−1)	8.07(−2)	2.6469	2.42(−1)	5.03(−2)
		$\frac{1}{2}$-$\frac{3}{2}$	*g*	2.6430	7.167(−4)	2.034(−1)	7.125(−2)	7.44(−4)	2.6431	6.4(−3)	8.07(−2)	2.6426	4.63(−4)	5.03(−2)
		$\frac{3}{2}$-$\frac{1}{2}$	*h*	2.6495	5.08(−3)	3.291(−1)	5.289(−3)	2.0(−4)	2.6493	4.48(−3)	3.96(−4)	2.6490	5.0(−3)	9.57(−4)
		$\frac{1}{2}$-$\frac{1}{2}$	*i*	2.6450	3.235(−1)	3.291(−1)	5.289(−3)	1.02(−2)	2.6451	3.12(−1)	3.96(−4)	2.6447	3.49(−1)	9.57(−4)
	$^2P^o$-^2D	$\frac{3}{2}$-$\frac{5}{2}$	*j*	2.6346	11.48	11.48	15.05	35.28	2.6355	12.4	14.4	2.6347	11.6	17.6
		$\frac{1}{2}$-$\frac{3}{2}$	*k*	2.6310	14.95	15.49	13.73	28.09	2.6326	15.8	13.8	2.6313	15.4	15.8
		$\frac{3}{2}$-$\frac{3}{2}$	*l*	2.6360	5.345(−1)	15.49	13.73	1.004	2.6368	1.74(−1)	13.8	2.6356	7.13(−1)	15.8
	$^2P^o$-^2S	$\frac{3}{2}$-$\frac{1}{2}$	*m*	2.6192	10.82	11.91	2.460	3.705	2.6198	11.6	1.87	2.6195	1.07(−1)	2.05(−1)
		$\frac{1}{2}$-$\frac{1}{2}$	*n*	2.6142	1.081	11.91	2.460	3.701(−1)	2.6157	1.13	1.87	2.6153	1.16	3.05
$1s^2 2p$-$1s\,2s^2$	$^2P^o$-^2S	$\frac{3}{2}$-$\frac{1}{2}$	*o*	2.6815	5.907(−1)	1.052	14.01	1.099	2.6740	7.98(−1)	13.4	2.6809	5.35(−1)	14.9
		$\frac{1}{2}$-$\frac{1}{2}$	*p*	2.6763	4.59(−1)	1.052	14.01	8.539(−1)	2.6697	6.6(−1)	13.4	2.6765	4.16(−1)	14.9
$1s^2 2s$-$1s\,2p\,2s$	^2S-$(^1P)^2P^o$	$\frac{1}{2}$-$\frac{3}{2}$	*q*	2.6270	23.63	23.64	1.027(−1)	4.090(−1)	2.6271	25.7	7.7(−2)	2.6272	24.0	2.68(−2)
		$\frac{1}{2}$-$\frac{1}{2}$	*r*	2.6297	17.30	17.31	2.448	4.288	2.6299	17.9	2.67	2.6294	18.3	2.08
	^2S-$(^3P)^2P^o$	$\frac{1}{2}$-$\frac{3}{2}$	*s*	2.6195	7.483(−1)	7.537(−1)	10.63	2.795	2.6207	7.34(−1)	10.3	2.6196	3.88(−1)	12.0
		$\frac{1}{2}$-$\frac{1}{2}$	*t*	2.6205	7.273	7.279	8.357	7.775	2.6214	8.79	7.72	2.6205	6.33	10.0
	^2S-$^4P^o$	$\frac{1}{2}$-$\frac{3}{2}$	*u*	2.6469	2.904(−1)	2.905(−1)	2.956(−2)	1.073(−1)	2.6464	3.45(−1)	2.09(−2)	2.6465	3.19(−1)	2.94(−2)
		$\frac{1}{2}$-$\frac{1}{2}$	*v*	2.6479	1.065(−1)	1.065(−1)	3.562(−3)	6.9(−3)	2.6479	1.46(−1)	1.68(−2)	2.6477	1.06(−1)	1.13(−2)

TABLE II. Atomic data related to the principal satellite lines of the $1s^2$-$1s\,2p$ Ti^{20+} resonance line due to transitions $1s^2nl$-$1s\,2l'nl''$ for $n=3$. The corrected wavelengths are in Å. A_r^{sf}, $\sum_{k<s} A_r^{sk}$, A_a^s, and $F_2(sf)$ are in units of 10^{13} s^{-1}.

Array	Multiplet	Key	Line	λ (Å)	A_r^{sf}	$\sum_{k<s} A_r^{sk}$	A_a^s	$F_2(sf)$
				(a)				
$1s^23s$-$1s\,2p\,3s$	^2S - $(^1P)^2P^o$	*a* 1	$\frac{1}{2}$-$\frac{3}{2}$	2.6126	20.46	21.23	3.785(−1)	1.434
		2	$\frac{1}{2}$-$\frac{1}{2}$	2.6122	19.79	20.39	1.187	2.176
	- $(^3P)^2P^o$	3	$\frac{1}{2}$-$\frac{3}{2}$	2.6169	3.108(−1)	5.404(−1)	4.154	1.100
		4	$\frac{1}{2}$-$\frac{1}{2}$	2.6208	3.519	3.763	3.650	3.465
	$^4P^o$	5	$\frac{1}{2}$-$\frac{3}{2}$	2.6266	6.598(−1)	1.090	4.642(−1)	1.078(−1)
-$1s\,2p\,3d$	^2S - $(^3P)^2D^o$	*b* 6	$\frac{1}{2}$-$\frac{3}{2}$	2.6150	7.696(−1)	2.236	3.452(−2)	4.7(−2)
-$1s\,2s\,3p$	^2S - $(^1S)^2P^o$	*c* 1	$\frac{1}{2}$-$\frac{3}{2}$	2.6222	8.283(−1)	3.956	2.607(−1)	2.048(−1)
$1s^23p$-$1s\,2p\,3p$	$^2P^o$ - $(^1P)^2S$	*d* 1	$\frac{3}{2}$-$\frac{1}{2}$	2.6098	15.37	18.03	1.232	1.966
		2	$\frac{1}{2}$-$\frac{1}{2}$	2.6093	2.224	18.03	1.232	2.845(−1)
	- $(^3P)^2S$	3	$\frac{3}{2}$-$\frac{1}{2}$	2.6176	7.111	12.93	2.431(−1)	2.625(−1)
	- $(^1P)^2P$	7	$\frac{1}{2}$-$\frac{3}{2}$	2.6129	20.24	21.82	3.286	11.16
	$(^3P)^2P$	11	$\frac{1}{2}$-$\frac{3}{2}$	2.6226	1.034	4.058	2.258(−1)	2.180(−1)
	$(^1P)^2D$	13	$\frac{3}{2}$-$\frac{5}{2}$	2.6139	21.08	22.35	3.510	17.17
		14	$\frac{3}{2}$-$\frac{3}{2}$	2.6127	21.35	24.15	1.331	4.462
	$(^3P)^2D$	16	$\frac{3}{2}$-$\frac{5}{2}$	2.6195	1.132	7.054	2.810	1.935
		17	$\frac{3}{2}$-$\frac{3}{2}$	2.6226	1.994	6.934	1.341	1.292
		18	$\frac{1}{2}$-$\frac{3}{2}$	2.6211	4.355(−1)	6.934	1.341	2.822(−1)
	^4S	19	$\frac{3}{2}$-$\frac{3}{2}$	2.6290	7.148(−1)	2.732	6.535(−2)	6.68(−2)
	^4P	21	$\frac{3}{2}$-$\frac{5}{2}$	2.6228	4.306(−1)	1.391	7.913(−2)	1.391(−1)
		22	$\frac{3}{2}$-$\frac{3}{2}$	2.6238	1.621(−1)	1.562	2.415(−2)	8.684(−2)
		24	$\frac{1}{2}$-$\frac{3}{2}$	2.6223	2.820(−1)	1.562	2.415(−2)	1.511(−2)
	^4D	26	$\frac{3}{2}$-$\frac{5}{2}$	2.6283	6.317(−1)	7.855(−1)	1.186(−1)	4.972(−1)
-$1s\,2s\,3s$	$^2P^o$ - $(^1S)^2S$	*e* 1	$\frac{3}{2}$-$\frac{1}{2}$	2.6366	9.522(−1)	1.876	2.301	1.049
		2	$\frac{1}{2}$-$\frac{1}{2}$	2.6350	6.132(−1)	1.876	2.301	6.756(−1)
-$1s\,2s\,3d$	$(^1S)^2D$	*f* 1	$\frac{3}{2}$-$\frac{5}{2}$	2.6235	1.265	1.952	2.651(−1)	9.075(−1)
$1s^23d$-$1s\,2p\,3d$	^2D - $(^1P)^2D^o$	*h* 7	$\frac{5}{2}$-$\frac{5}{2}$	2.6120	16.36	25.05	1.400(−1)	5.458(−1)
		9	$\frac{3}{2}$-$\frac{5}{2}$	2.6116	7.232	25.05	1.400(−1)	2.413(−1)
	- $(^1P)^2F^o$	15	$\frac{5}{2}$-$\frac{7}{2}$	2.6111	19.44	20.91	1.438	10.00
		16	$\frac{5}{2}$-$\frac{5}{2}$	2.6098	12.74	20.56	1.321	4.616
		17	$\frac{3}{2}$-$\frac{5}{2}$	2.6102	6.195	20.56	1.321	2.244
	- $(^3P)^2F^o$	18	$\frac{5}{2}$-$\frac{7}{2}$	2.6188	4.706	5.394	1.016(−2)	7.076(−2)
	- $^4F^o$	32	$\frac{5}{2}$-$\frac{7}{2}$	2.6260	4.623(−1)	6.597(−1)	3.560(−2)	1.893(−1)
		35	$\frac{3}{2}$-$\frac{5}{2}$	2.6271	6.626(−1)	8.611(−1)	2.102(−2)	9.473(−2)

tation as Gabriel.[3] In Table II, only those lines with $n=3$ and 4, which have values of $F_2(sf)$ greater than 1.10^{12} and 5.10^{11} s^{-1}, respectively, are shown. All the wavelengths generated were "normalized" to an assumed resonance-line wavelength of 2.6099 Å, using a double-difference correction described by Bely-Dubau *et al.*[11] For Ti^{19+}, this gives a correction factor of $\Delta\lambda = +0.0025$ Å. Table I also shows

TABLE II. (*Continued.*)

Array	Multiplet	Key	Line	λ (Å)	A_r^{sf}	$\sum_{k<s} A_r^{sk}$	A_a^s	$F_2(sf)$
			(b) As in (a) for $n=4$					
$1s^24s$-$1s2p4s$	^2S -$(^1P)^2P^o$	j 1	$\frac{1}{2}$-$\frac{3}{2}$	2.6107	23.37	23.56	3.463(−2)	1.372(−1)
		2	$\frac{1}{2}$-$\frac{1}{2}$	2.6107	23.10	23.27	2.019(−1)	3.994(−1)
	$(^3P)^2P^o$	3	$\frac{1}{2}$-$\frac{3}{2}$	2.6183	2.332(−2)	2.443(−1)	1.166	7.713(−2)
	$^4P^o$	5	$\frac{1}{2}$-$\frac{3}{2}$	2.6238	1.014	1.185	2.682(−2)	8.976(−2)
-$1s2s4p$	^2S -$(^1S)^2P^o$	l 1	$\frac{1}{2}$-$\frac{3}{2}$	2.6217	1.168(−1)	1.159	5.523(−1)	1.508(−1)
		2	$\frac{1}{2}$-$\frac{1}{2}$	2.6218	1.040	1.434	1.648	1.112
$1s^24p$-$1s2p4p$	$^2P^o$-$(^1P)^2S$	m 1	$\frac{3}{2}$-$\frac{1}{2}$	2.6102	19.65	23.74	4.518(−1)	7.338(−1)
		2	$\frac{1}{2}$-$\frac{1}{2}$	2.6095	3.637	23.74	4.518(−1)	1.358(−1)
	$(^3P)^2S$	3	$\frac{3}{2}$-$\frac{1}{2}$	2.6179	7.285(−1)	3.073	3.426(−1)	1.461(−1)
	$(^1P)^2P$	7	$\frac{1}{2}$-$\frac{3}{2}$	2.6110	23.25	24.09	1.144	4.218
	$(^3P)^2P$	9	$\frac{3}{2}$-$\frac{3}{2}$	2.6199	2.637(−1)	1.663	2.842(−1)	1.539(−1)
	$(^1P)^2D$	13	$\frac{3}{2}$-$\frac{5}{2}$	2.6113	23.69	24.70	8.774(−1)	4.876
		14	$\frac{3}{2}$-$\frac{3}{2}$	2.6116	23.46	24.61	3.291(−1)	1.239
	$(^3P)^2D$	17	$\frac{3}{2}$-$\frac{3}{2}$	2.6246	2.688(−1)	1.654	9.019(−2)	5.560(−2)
		18	$\frac{1}{2}$-$\frac{3}{2}$	2.6240	5.630(−1)	1.654	9.019(−2)	1.164(−1)
	^4P	22	$\frac{3}{2}$-$\frac{3}{2}$	2.6230	7.953(−1)	3.208	8.504(−1)	6.667(−1)
		24	$\frac{1}{2}$-$\frac{3}{2}$	2.6223	3.336(−1)	3.208	8.504(−1)	2.796(−1)
	^4D	26	$\frac{3}{2}$-$\frac{5}{2}$	2.6242	8.658(−1)	1.078	2.132(−1)	8.582(−1)
		29	$\frac{1}{2}$-$\frac{3}{2}$	2.6247	4.232(−1)	6.207(−1)	6.157(−2)	1.528(−1)
-$1s2s4s$	$^2P^o$-$(^1S)^2S$	o 1	$\frac{3}{2}$-$\frac{1}{2}$	2.6279	4.257(−1)	8.227(−1)	8.113(−1)	4.227(−1)
		2	$\frac{1}{2}$-$\frac{1}{2}$	2.6272	2.698(−1)	8.227(−1)	8.113(−1)	2.679(−1)
-$1s2s4d$	$^2P^o$-$(^1S)^2D$	p 1	$\frac{3}{2}$-$\frac{5}{2}$	2.6226	1.153(−1)	6.322(−1)	5.794(−2)	5.808(−2)
$1s^24d$-$1s2p4s$	^2D -$(^3P)^2P^o$	q 5	$\frac{3}{2}$-$\frac{3}{2}$	2.6224	6.130(−2)	2.443(−1)	1.166	2.027(−1)
-$1s2p4d$	^2D -$(^1P)^2P^o$	r 1	$\frac{5}{2}$-$\frac{3}{2}$	2.6094	22.28	24.22	2.341(−2)	8.606(−2)
	$(^1P)^2D^o$	7	$\frac{5}{2}$-$\frac{5}{2}$	2.6106	13.31	24.45	1.329(−1)	4.316(−1)
		9	$\frac{3}{2}$-$\frac{5}{2}$	2.6104	10.60	24.45	1.329(−1)	3.437(−1)
	$(^1P)^2F^o$	15	$\frac{5}{2}$-$\frac{7}{2}$	2.6105	23.72	24.08	6.878(−1)	5.270
		16	$\frac{5}{2}$-$\frac{5}{2}$	2.6101	10.31	23.37	6.265(−1)	1.615
		17	$\frac{3}{2}$-$\frac{5}{2}$	2.6100	12.53	23.37	6.265(−1)	1.963
	$(^3P)^2F^o$	18	$\frac{5}{2}$-$\frac{7}{2}$	2.6181	2.576(−1)	8.842(−1)	6.135(−2)	1.337(−1)
	$^4D^o$	30	$\frac{3}{2}$-$\frac{3}{2}$	2.6225	5.468(−1)	1.074	9.735(−2)	1.818(−1)
	$^4F^o$	32	$\frac{5}{2}$-$\frac{7}{2}$	2.6231	6.556(−1)	9.746(−1)	4.707(−2)	2.416(−1)
-$1s2s4p$	^2D -$(^1S)^3P$	s 1	$\frac{5}{2}$-$\frac{3}{2}$	2.6259	2.444(−1)	1.159	5.523(−1)	3.155(−1)
		3	$\frac{3}{2}$-$\frac{1}{2}$	2.6259	7.065(−2)	1.434	1.648	7.556(−2)
$1s^24f$-$1s2p4f$	$^2F^o$-$(^1P)^2G$	u 15	$\frac{7}{2}$-$\frac{9}{2}$	2.6094	23.88	24.10	4.507(−2)	4.457(−1)
		17	$\frac{5}{2}$-$\frac{7}{2}$	2.6093	22.23	23.98	4.708(−2)	3.486(−1)
	^4F	30	$\frac{5}{2}$-$\frac{5}{2}$	2.6218	8.573(−1)	1.205	3.381(−2)	1.404(−1)

the comparison with some earlier calculations for $n=2$.[18,19] The agreement is good for the wavelengths, but there are some significant changes in the autoionizing rates of Vainshtein and Safronova, differences which have previously been noted and discussed in previous papers.[15,17]

III. INNER-SHELL EXCITED SATELLITE LINES

This alternative method for exciting satellite lines is important only for $n=2$. Some satellite lines (e.g., "q" as defined in Table I) are produced mainly by inner-shell excitation and their ratio to the resonance line gives primarily the Ti^{19+} to Ti^{20+} ion ratio, whereas the electronic temperature is determined from the pure dielectronic satellite line.[3] In addition to the above derived atomic parameters, it is thus necessary to have values of the collisional excitation rate for each level. The atomic data necessary to obtain these excitation rates have been calculated using the programs SUPERSTRUCTURE,[16] DISTORTED WAVE,[20] and JJOM.[21,22] The details of the method have been described by Bely-Dubau *et al.*[13,14] To be consistent with the previous calculations we used the same values of λ in the programs mentioned above. As already mentioned by Bely-Dubau *et al.*[14] the collision strengths obtained are in good agreement with those of Sampson *et al.*[23] The results for the excitation rates are given in Table III for the $n=2$ satellite lines for a large range of temperatures.

IV. EXCITATION OF HELIUMLIKE Ti^{20+}

The excitation rates of the heliumlike lines have been calculated using the same methods as for the inner-shell excited satellite lines. The results given in Table IV do not take into account the effect of cascades and of autoionizing resonances. These processes can be very important, in particular, for the line z. However, in this paper, we are interested in the interpretation of spectra of titanium near the heliumlike resonance line, and the two processes mentioned above are negligible for this line. As in the Li-like case (Sec. III) the collision strengths obtained are in good agreement with those of Sampson *et al.*[24]

TABLE III. Electron excitation rates C ($cm^3\ s^{-1}$) from the ground state $1s^2 2s\ ^2S$ of Ti^{19+}.

$T(10^6$ K)	$1s2s^2\,^2S_{1/2}$	$1s2s2p\,^4P_{1/2}$	$1s2s2p\,^4P_{3/2}$	$1s2s2p\,^4P_{5/2}$	$^2P_{1/2}(r)$	$^2P_{3/2}(q)$	$^2P_{1/2}(t)$	$^2P_{1/2}(s)$
2.5	0.129(−20)	0.596(−21)	0.120(−20)	0.170(−20)	0.136(−20)	0.332(−20)	0.782(−21)	0.988(−21)
3	0.438(−19)	0.201(−19)	0.408(−19)	0.579(−19)	0.484(−19)	0.118(−18)	0.279(−19)	0.348(−19)
3.5	0.537(−18)	0.245(−18)	0.498(−18)	0.709(−18)	0.615(−18)	0.151(−17)	0.354(−18)	0.437(−18)
4	0.349(−17)	0.158(−17)	0.322(−17)	0.458(−17)	0.412(−17)	0.102(−16)	0.236(−17)	0.288(−17)
5	0.472(−16)	0.209(−16)	0.429(−16)	0.611(−16)	0.584(−16)	0.145(−15)	0.332(−16)	0.396(−16)
6	0.264(−15)	0.114(−15)	0.236(−15)	0.335(−15)	0.339(−15)	0.845(−15)	0.191(−15)	0.222(−15)
7	0.891(−15)	0.379(−15)	0.783(−15)	0.111(−14)	0.118(−14)	0.296(−14)	0.659(−15)	0.749(−15)
8	0.220(−14)	0.918(−15)	0.190(−14)	0.270(−14)	0.302(−14)	0.756(−14)	0.166(−14)	0.184(−14)
9	0.442(−14)	0.181(−14)	0.375(−14)	0.532(−14)	0.623(−14)	0.156(−13)	0.338(−14)	0.368(−14)
10	0.769(−14)	0.308(−14)	0.641(−14)	0.907(−14)	0.111(−13)	0.280(−13)	0.596(−14)	0.634(−14)
11	0.120(−13)	0.473(−14)	0.987(−14)	0.139(−13)	0.178(−13)	0.449(−13)	0.946(−14)	0.984(−14)
12	0.174(−13)	0.672(−14)	0.140(−13)	0.198(−13)	0.263(−13)	0.666(−13)	0.139(−13)	0.141(−13)
13	0.238(−13)	0.899(−14)	0.188(−13)	0.265(−13)	0.366(−13)	0.928(−13)	0.191(−13)	0.191(−13)
14	0.309(−13)	0.115(−13)	0.241(−13)	0.338(−13)	0.486(−13)	0.123(−12)	0.251(−13)	0.246(−13)
15	0.388(−13)	0.142(−13)	0.298(−13)	0.416(−13)	0.621(−13)	0.158(−12)	0.319(−13)	0.306(−13)
17	0.560(−13)	0.198(−13)	0.417(−13)	0.581(−13)	0.930(−13)	0.237(−12)	0.469(−13)	0.433(−13)
20	0.838(−13)	0.282(−13)	0.599(−13)	0.826(−13)	0.146(−12)	0.374(−12)	0.722(−13)	0.632(−13)
25	0.130(−12)	0.406(−13)	0.870(−13)	0.119(−12)	0.243(−12)	0.626(−12)	0.117(−12)	0.944(−13)
30	0.172(−12)	0.502(−13)	0.150(−12)	0.146(−12)	0.342(−12)	0.883(−12)	0.161(−12)	0.120(−12)
35	0.208(−12)	0.570(−13)	0.167(−12)	0.165(−12)	0.435(−12)	0.113(−11)	0.201(−12)	0.141(−12)
40	0.237(−12)	0.616(−13)	0.177(−12)	0.177(−12)	0.521(−12)	0.136(−11)	0.237(−12)	0.157(−12)
45	0.262(−12)	0.644(−13)	0.184(−12)	0.185(−12)	0.600(−12)	0.157(−11)	0.270(−12)	0.170(−12)
50	0.282(−12)	0.660(−13)	0.187(−12)	0.188(−12)	0.672(−12)	0.176(−11)	0.299(−12)	0.179(−12)
60	0.311(−12)	0.668(−13)	0.188(−12)	0.188(−12)	0.795(−12)	0.209(−11)	0.348(−12)	0.192(−12)
80	0.343(−12)	0.636(−13)	0.179(−12)	0.176(−12)	0.979(−12)	0.259(−11)	0.420(−12)	0.202(−12)
100	0.355(−12)	0.586(−13)	0.167(−12)	0.158(−12)	0.111(−11)	0.295(−11)	0.467(−12)	0.205(−12)

TABLE IV. Electron excitation rates C ($cm^2 s^{-1}$) from the ground state $1s^2\,{}^1S_0$ of Ti^{20+}.

$T(10^6$ K)	$1s2s\,{}^3S_1$	$1s2p\,{}^3P_0$	$1s2s\,{}^1S_0$	$1s2p\,{}^3P_1$	$1s2p\,{}^3P_2$	$1s2p\,{}^1P_1$
2.5	0.804(−21)	0.438(−21)	0.137(−20)	0.149(−20)	0.219(−20)	0.431(−20)
3	0.277(−19)	0.154(−19)	0.490(−19)	0.523(−19)	0.770(−19)	0.158(−18)
3.5	0.343(−18)	0.193(−18)	0.623(−18)	0.656(−18)	0.966(−18)	0.205(−17)
4	0.224(−17)	0.127(−17)	0.417(−17)	0.433(−17)	0.636(−17)	0.139(−16)
5	0.303(−16)	0.174(−16)	0.588(−16)	0.594(−16)	0.870(−16)	0.202(−15)
6	0.168(−15)	0.974(−16)	0.339(−15)	0.334(−15)	0.487(−15)	0.119(−14)
7	0.564(−15)	0.326(−15)	0.117(−14)	0.113(−14)	0.163(−14)	0.422(−14)
8	0.138(−14)	0.800(−15)	0.296(−14)	0.278(−14)	0.400(−14)	0.109(−13)
9	0.274(−14)	0.159(−14)	0.605(−14)	0.555(−14)	0.795(−14)	0.226(−13)
10	0.470(−14)	0.272(−14)	0.107(−13)	0.958(−14)	0.136(−13)	0.405(−13)
11	0.727(−14)	0.422(−14)	0.169(−13)	0.149(−13)	0.211(−13)	0.653(−13)
12	0.104(−13)	0.600(−14)	0.248(−13)	0.214(−13)	0.300(−13)	0.971(−13)
13	0.140(−13)	0.808(−14)	0.342(−13)	0.289(−13)	0.404(−13)	0.136(−12)
14	0.180(−13)	0.104(−13)	0.450(−13)	0.373(−13)	0.518(−13)	0.181(−12)
15	0.223(−13)	0.128(−13)	0.569(−13)	0.464(−13)	0.639(−13)	0.232(−12)
17	0.314(−13)	0.179(−13)	0.836(−13)	0.659(−13)	0.896(−13)	0.305(−12)
20	0.453(−13)	0.256(−13)	0.128(−12)	0.964(−13)	0.128(−12)	0.554(−12)
25	0.663(−13)	0.372(−13)	0.205(−12)	0.144(−12)	0.186(−12)	0.934(−12)
30	0.829(−13)	0.460(−13)	0.277(−12)	0.185(−12)	0.230(−12)	0.132(−11)
35	0.951(−13)	0.520(−13)	0.341(−12)	0.217(−12)	0.260(−12)	0.170(−11)
40	0.104(−12)	0.562(−13)	0.397(−12)	0.243(−12)	0.281(−12)	0.205(−11)
45	0.109(−12)	0.586(−13)	0.444(−12)	0.262(−12)	0.293(−12)	0.237(−11)
50	0.112(−12)	0.600(−13)	0.484(−12)	0.277(−12)	0.300(−12)	0.266(−11)
60	0.114(−12)	0.602(−13)	0.546(−12)	0.298(−12)	0.301(−12)	0.317(−11)
80	0.110(−12)	0.564(−13)	0.622(−12)	0.317(−12)	0.282(−12)	0.394(−11)
100	0.101(−12)	0.510(−13)	0.660(−12)	0.322(−12)	0.255(−12)	0.448(−11)

V. CLOSE SATELLITE LINES

Dielectronic satellite lines with increasing n will form series which converge on their parent He-like line. The importance of the contribution of these higher-n satellites to the resonance line has been shown by Bely-Dubau *et al.*[12] for Fe^{24+}. To estimate this contribution we use a method of extrapolation described in Bely-Dubau *et al.*[13,14] The satellite lines with $n>4$ are extrapolated line by line from a selected set of lines corresponding to $n=4$ using the following assumptions:

(I) $$A_r^{sf}(n>4)=\sum_{k<s} A_r^{sk} = A_{\rm res} = 2.427\times 10^{14}\ {\rm s}^{-1}\ ,$$

(II) $A_a \propto n^{-3}$,

(III) the wavelength difference between each satellite line and its parent line varies as n^{-3}.

For the satellite lines to the Ti^{20+} resonance line the extrapolated series is truncated at $n=10$. Above this value of n, the levels can be autoionized to a new continuum ($1s2s\,{}^3S+e$), and this process decreases the intensity of the satellite lines due to these levels. The importance of the close satellites will be discussed in Sec. VI where their effects will be incorporated in the analysis of the experimental spectrum.

VI. LINE FITTING OF THE Ti^{20+} SPECTRUM

A dielectronic satellite spectrum of Ti^{20+} was observed from ohmically heated PDX tokamak discharges with central electron temperatures of ≈ 1 keV by means of a high-resolution ($\lambda/\Delta\lambda=23\,000$ at $\lambda=2.6099$-Å) Bragg curved crystal spectrometer. Figure 1 shows the spectrum which covers a spectral range from 2.6050 to 2.6320 Å. Theoretical results from Tables I and II enable all the important spectral features to be identified. With this set of data we attempt to fit the spectrum shown in Fig. 1 near the Ti^{20+} resonance line w between 2.6050 and 2.6150 Å. In addition to the line w, this range includes all the satellite lines with $n>2$. From Table III, we selected the transitions which fall in this

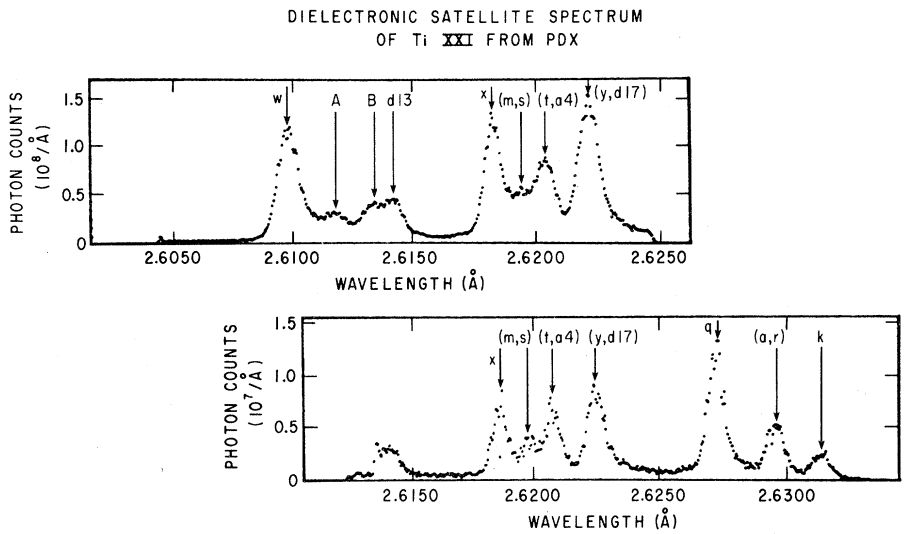

FIG. 1. Satellite spectrum of Ti^{20+}.

wavelength range. These are 13 ($n=3$) and 14 ($n=4$) satellites. For these transitions and for the resonance line w, Voigt profiles were calculated. The Doppler and electron temperatures T_D and T_e were adjusted to obtain the best fit with the experimental data. In order to obtain good agreement between the theoretical and experimental wavelengths, it was necessary to increase the former wavelengths by $\Delta\lambda=0.0005$ Å for the line $d13$ and $\Delta\lambda=0.0007$ Å for the features "A" and "B". This correction is

TABLE V. (a) Wavelengths in Å and line factors $F_2(sf)$ in 10^{13} s^{-1} for the principal lines of the $n=5$ complex, extrapolated from the corrected wavelengths of the $n=4$ complex (see text). (b) Wavelengths in Å and line factors $\langle F_2(sf)\rangle$ in 10^{13} s^{-1} for the $n>6$ blended satellite lines (see text).

$n=4$		$n=5$	
λ_{corr}	Key	λ_{ext}	$F_2(sf)$
	(a)		
2.6114	j 1	2.6107	7.075(−2)
2.6114	j 2	2.6107	2.071(−1)
2.6107	m 1	2.6103	4.576(−1)
2.6117	m 7	2.6108	2.289
2.6120	m 13	2.6110	2.645
2.6121	m 14	2.6110	6.674(−1)
2.6099	r 1	2.6099	4.798(−2)
2.6109	r 9	2.6104	4.069(−1)
2.6110	r 15	2.6105	2.776
2.6106	r 16	2.6103	1.901
2.6099	u 15	2.6099	2.308(−1)
2.6098	u 17	2.6099	1.926(−1)

λ(Å)	$\langle F_2(sf)\rangle$
(b)	
2.6099	5.4368
2.6100	3.4543
2.6101	3.7432
2.6102	1.6060
2.6103	1.4857
2.6104	0.3862
2.6106	1.5310

within the order of validity of the program SUPERSTRUCTURE. From the wavelengths adopted for the $n=4$ satellite lines, we extrapolated the values of the satellite lines with $n=5-10$ according to the assumptions of Sec. V. The results for the $n=5$ satellites are given in Table V(a).

The data for the $n>6$ satellites, which are located in a range very close to the resonance line ($\Delta\lambda<0.0006$ Å), are summarized in Table V(b). $\langle F_2(sf)\rangle$ represents the sum of the line factors of these satellites at a given wavelength. In this form the data can be easily used to evaluate the intensity contribution from these satellites, if one approximates in the expression $F_1(T_e)$ given in Eq. (2.2) the energy E_s for each $n>6$ satellite line by $\bar{E}_s(n=6)$, i.e., $E_s=4.602$ keV.

Comparison between experiment and theory is given in Figs. 2(a) and 2(b). Figure 2(a) presents experimental results and the theoretical predictions for the resonance line (w) and the $n=3$ and $n=4$ satellites (curve II) as calculated from the data in Tables II(a) and II(b). The theoretical curves shown in Fig. 2(b) also include the contribution from the satellites with $n=5-10$ (curve III) and incorporate the described corrections of the theoretical wavelengths. Curve III represents 11 Voigt functions which have been calculated from the data given in Tables V(a) and V(b). The theoretical curves have been calculated assuming ion and electron temperatures of $T_D=0.8$ keV and $T_e=0.9$ keV. For these temperature values we obtained the best fit to the experimental data.

The experimental data as shown in Figs. 2(a) and 2(b) have been corrected for geometrical effects, because the size of the beryllium window on the PDX tokamak limited the solid angle for spectral lines in the considered wavelength range. This window effect is represented by a trapezoidal function which increases the line intensities around line x relative to w. The slope of this trapezoidal function can be determined from geometrical considerations. It can also be inferred from the difference of the backgrounds observed in Fig. 1 between the lines $d13$ and x (at 2.6165 Å) and the short-wavelength side of w (at 2.6050 Å). Previously observed spectra[9] of heliumlike iron Fe^{24+} show no difference in the background of the corresponding spectral regions.

It is interesting to determine the effect of the unresolved satellites on the "apparent" resonance-line profile [curve I, in Fig. 2(b)]. The peak of curve I is shifted with respect to the peak of w by an amount $\Delta\lambda=5.5\times10^{-5}$ Å. The full width at half maximum, (FWHM) of the apparent resonance line is 9.8×10^{-4} Å, whereas the width (FWHM) of the true resonance line is 8.7×10^{-4} Å. However, the profile of curve I is asymmetric. Its halfwidth on the short-wavelength side is practically the same as the halfwidth of w. This is of importance for ion-temperature measurements. A detailed discussion has been given in a previous paper.[9] Differences in the widths of the "apparent" and the "true" resonance-line profiles, of course, disappear with increasing electron temperature.

Ion- and electron-temperature results for the

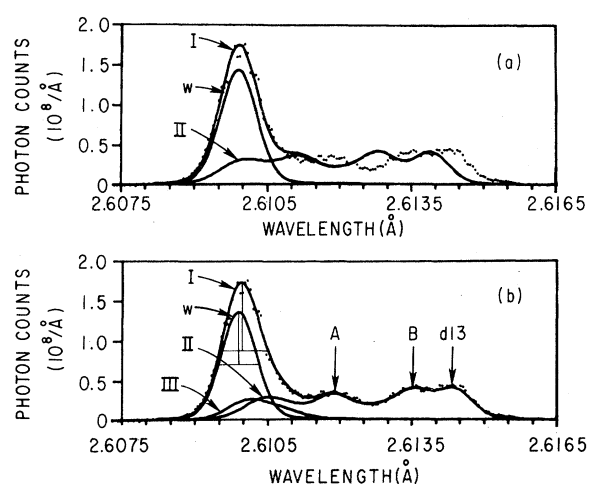

FIG. 2. Experimental spectrum near the resonance line of Ti^{20+} compared with the synthetic spectrum (curve I) computed using the present theory and assuming $T_e=0.9$ keV and $T_D=0.8$ keV: (a) from the data in Tables II(a) and II(b); (b) with the corrected wavelengths (see text). The curves w, II, and III show contributions from the resonance line, the satellite lines with $n=3$, 4, and the satellite lines with $n=5-10$, respectively.

TABLE VI. Contribution $\alpha(T_e)$ of the unresolved satellite lines to the w resonance line of Ti^{20+} with a spectral resolution of $\lambda/\Delta\lambda=3700$.

$T(10^6$ K)	3	3.5	4	5	6	7	8	9
α	3.43	2.30	1.69	1.06	0.751	0.570	0.452	0.374
$T(10^6$ K)	10	11	12	13	14	15	17	20
α	0.316	0.272	0.237	0.209	0.187	0.168	0.139	0.108

same PDX discharges have been obtained from measurements of charge-exchange neutrals and observation of the soft-x-ray bremsstrahlung spectrum. These results are in agreement with the values of T_D and T_e as deduced from the fit in Fig. 2(b) to within 100 eV. This can be considered as an experimental confirmation of our theory.

For many diagnostic applications one is interested in evaluation of satellite intensities relative to the resonance line, rather than in a detailed analysis of the apparent resonance-line profile. For these purposes it is only necessary to know the apparent intensity increase $\Delta I_w=\alpha(T_e)I_w$ of the resonance line due to unresolved satellites. We have therefore calculated

$$\alpha=\sum_s \frac{I_{sf}}{I_w}$$

(where I_w is the intensity of the resonance line due to direct excitation) for a spectral resolution of $\lambda/\Delta\lambda=3700$, which corresponds to a Doppler resolution at 15×10^6 K. The results are given in Table VI as a function of electron temperature. It is evident that this contribution must be taken into account for evaluation of intensity ratios.

VII. CONCLUSION

New calculations for the wavelengths and atomic parameters have been carried out using a coherent set of methods for both the dielectronic and inner-shell satellite lines of the Ti^{20+} resonance line. There is a good agreement with existing calculations for the $n=2$ lines. These data were used to fit an experimental spectrum obtained from PDX tokamak discharges by means of a high-resolution Bragg curved crystal spectrometer. The comparison between theoretical and experimental wavelengths allows for a small correction for the $n>2$ satellite-line wavelengths, near the resonance line w. With this correction, quite good agreement between theoretical and experimental results is obtained. The Doppler and electron temperatures thus deduced compare very well with those obtained from other methods.

Some modifications of the spectrometer would enable us to obtain a broader spectral band. We plan to calculate a complete data set including processes mentioned above for several ionization stages of titanium (Ti^{18+}, Ti^{19+}, Ti^{20+}) in order to obtain a complete line fitting of the Ti broadband spectrum.

ACKNOWLEDGMENTS

Parts of this work were supported by the United States Department of Energy, Contract No. DE-AC02-76-CHO-3073, and a grant from NATO.

[1]A. H. Gabriel, C. Jordan, and T. M. Paget, *Proceedings of the 6th International Conference on Physics of Electronic and Atomic Collisions* (MIT, Cambridge, Massachusetts, 1969), p. 558.

[2]A. H. Gabriel and T. M. Paget, J. Phys. B 5, 673 (1972).

[3]A. H. Gabriel, Mon. Not. R. Astron. Soc. 160, 99 (1972).

[4]J. H. Parkinson, Nature Phys. Sci. 236, 68 (1972).

[5]Y. I. Grineva, V. I. Karov, V. V. Korneev, V. V. Krutov, S. L. Mandelstam, L. A. Vainshtein, B. N. Vasilysev, and J. A. Zhitnik, Sol. Phys. 29, 441 (1973).

[6]G. A. Doschek, R. W. Kreplin, and U. Feldman, Astrophys. J. 233, L157 (1979).

[7]A. H. Gabriel, J. L. Culhane, L. W. Acton, E. Antonucci, R. D. Bentley, C. Jordan, L. W. Leibacher, A. N. Parmar, K. J. H. Phillips, C. G. Rapley, C. J. Wolfson, and K. T. Strong, Adv. Space Res. 1, 267 (1981).

[8]M. Bitter, K. W. Hill, N. R. Sauthoff, P. C. Efthimion, E. Meservey, W. Roney, S. von Goeler, R. Horton, M. Goldman, and W. Stodiek, Phys. Rev. Lett. 43, 129 (1979).

[9]M. Bitter, S. von Goeler, K. W. Hill, R. Horton, D. Johnson, W. Roney, N. Sauthoff, E. Silver, and W. Stodiek, Phys. Rev. Lett. 47, 921 (1981).

[10]T. F. R. Group, J. Dubau, M. Loulergue, J. Phys. B 15, 1007 (1982).
[11]F. Bely-Dubau, A. H. Gabriel, and S. Volonté, Mon. Not. R. Astron. Soc. 186, 405 (1979).
[12]F. Bely-Dubau, A. H. Gabriel, and S. Volonté, Mon. Not. R. Astron. Soc. 189, 801 (1979).
[13]F. Bely-Dubau, J. Dubau, P. Faucher, and L. Steenman-Clark, J. Phys. B 14, 3313 (1981).
[14]F. Bely-Dubau, J. Dubau, P. Faucher, and A. H. Gabriel, Mon. Not. R. Astron. Soc. 198, 239 (1982).
[15]J. Dubau, M. Loulergue, and L. Steenman-Clark, Mon. Not. R. Astron. Soc. 190, 125 (1980).
[16]W. Eissner, M. Jones, and H. Nussbaumer, Comput. Phys. Commun. 8, 270 (1974).
[17]L. Steenman-Clark, F. Bely-Dubau, and P. Faucher, Mon. Not. R. Astron. Soc. 191, 951 (1980).
[18]C. P. Bhalla, A. H. Gabriel, and L. P. Presnyakov, Mon. Not. R. Astron. Soc. 172, 359 (1975).
[19]L. A. Vainshtein and U. I. Safronova, At. Data Nucl. Data Tables 21, 49 (1978).
[20]W. Eissner and M. J. Seaton, J. Phys. B 5, 2187 (1972).
[21]H. E. Saraph, Comput. Phys. Commun. 3, 256 (1972).
[22]H. E. Saraph, Comput. Phys. Commun. 15, 247 (1978).
[23]D. H. Sampson, R. E. H. Clark, and A. D. Parks, Phys. Rev. A 12, 3257 (1979).
[24]D. H. Sampson, A. D. Parks, and R. E. H. Clark, Phys. Rev. A 17, 1619 (1978).